References

1 Dillon S R, Sprecher C, Hammond A *et al.* Nat Immunol 2004: **5**: 752–760.
2 Takaoka A, Arai I, Sugimoto M *et al.* Er J Pharmacol 2005: **516**: 180–181.
3 Takaoka A, Arai I, Sugimoto M *et al.* Exp Dermatol 2006: **15**: 161–167.
4 Matsuda H, Watanabe N, Gregory P G *et al.* Int Immunol 1997: **9**: 461–466.
5 Yamaguchi T, Maekawa T, Nishikawa Y *et al.* J Dermatol Sci 2001: **25**: 20–28.
6 Grimstad O, Sawanobori Y, Vestergaard C *et al.* Exp Dermatol 2009: **18**: 35–43.
7 Sonkoly E, Muller A, Lauerma A I *et al.* J Allergy Clin Immunol 2006: **117**: 411–417.
8 Bilsborough J, Leung D Y, Maurer M *et al.* J Allergy Clin Immunol 2006: **117**: 418–425.
9 Ezzat M H, Hasan Z E, Shaheen K Y. J Eur Acad Dermatol Venereol 2011: **25**: 334–339.
10 Raap U, Weißmantel S, Gehring M *et al.* Pediatr Allergy Immunol 2012: **23**: 285–288.
11 Kim S, Kim H J, Yang H S *et al.* Ann Dermatol 2011: **23**: 468–473.
12 Szegedi K, Kremer A E, Kezic S *et al.* Exp Dermatol 2012: **21**: 431–6.
13 Cevikbas F, Wang X, Akiyama T *et al.* J Allergy Clin Immunol 2014: **133**: 448–60.
14 Akiyama N, Ohno Y, Fukuda T *et al.* BBRC 2009: **381**: 612–618.
15 Arai I, Tsuji M, Takeda H *et al.* Exp Dermatol 2013: **22**: 669–671.
16 Inagaki N, Igeta K, Shiraishi N *et al.* MicroAct Skin Pharmacol Appl Skin Physiol 2003: **16**: 165–175.
17 Takano N, Arai I, Kurachi M. Eur J Pharmacol 2003: **471**: 223–228.
18 Takano N, Arai I, Hashimoto Y *et al.* Eur J Pharmacol 2004: **495**: 159–165.
19 Hashimoto Y, Arai I, Takano N *et al.* Br J Dermatol 2006: **154**: 28–33.
20 Takaoka A, Arai I, Sugimoto M *et al.* Exp Dermatol 2007: **16**: 331–339.

Supporting Information

Additional supporting data may be found in the supplementary information of this article.

Data S1. Purified mIL-31 from culture supernatants from transfected Free Style 293 cells was glycosylated. Western blotting analysis with Anti-H6 antibody or anti-IL-31 rabbit polyclonal antibodies showed the same staining pattern, although western blotting analysis is a semi-quantitative assay. Taken together, these results suggested that this purification method excluded most contaminants other than IL-31.

DOI: 10.1111/exd.12553
www.wileyonlinelibrary.com/journal/EXD

Methods Letter to the Editor

An automated image processing method to quantify collagen fibre organization within cutaneous scar tissue

Kyle P. Quinn[1], Alexander Golberg[2,3], G. Felix Broelsch[4], Saiqa Khan[4], Martin Villiger[5], Brett Bouma[5], William G. Austen Jr[4], Robert L. Sheridan[6], Martin C. Mihm Jr[7], Martin L. Yarmush[2,8] and Irene Georgakoudi[1]

[1]Department of Biomedical Engineering, Tufts University, Medford, MA, USA; [2]Center for Engineering in Medicine, Department of Surgery, Massachusetts General Hospital, Harvard Medical School, and the Shriners Burns Hospital, Boston, MA, USA; [3]Porter School of Environmental Studies, Tel Aviv University, Ramat-Aviv, Tel Aviv, Israel; [4]Division of Plastic and Reconstructive Surgery, Massachusetts General Hospital, Harvard Medical School, Boston, MA, USA; [5]Wellman Center for Photomedicine, Massachusetts General Hospital, Boston, MA, USA; [6]Sumner Redstone Burn Center, Shriners Hospital for Children, Boston, MA, USA; [7]Department of Dermatology, Brigham and Women's Hospital, Harvard Medical School, Boston, MA, USA; [8]Department of Biomedical Engineering, Rutgers University, Piscataway, NJ, USA
Correspondence: Kyle P. Quinn, PhD, Department of Biomedical Engineering, Tufts University, 4 Colby Street, Medford, MA 02155, USA, Tel.: 608-347-8890, Fax: 617-627-3231, e-mail: kyle@quinnlab.org

Abstract: Standard approaches to evaluate scar formation within histological sections rely on qualitative evaluations and scoring, which limits our understanding of the remodelling process. We have recently developed an image analysis technique for the rapid quantification of fibre alignment at each pixel location. The goal of this study was to evaluate its application for quantitatively mapping scar formation in histological sections of cutaneous burns. To this end, we utilized directional statistics to define maps of fibre density and directional variance from Masson's trichrome-stained sections for quantifying changes in collagen organization during scar remodelling. Significant increases in collagen fibre density are detectable soon after burn injury in a rat model. Decreased fibre directional variance in the scar was also detectable between 3 weeks and 6 months after injury, indicating increasing fibre alignment. This automated analysis of fibre organization can provide objective surrogate endpoints for evaluating cutaneous wound repair and regeneration.

Key words: burns – collagen – fibre alignment – image analysis – scar remodelling

Accepted for publication 21 September 2014

Background

Evaluating collagen fibre organization in the dermis is critical to diagnosing disease, assessing the status of healing wounds and characterizing tissue regeneration (1–5). However, to evaluate this organization, standard approaches rely on qualitative descriptions or subjective scoring systems, which prevent comparisons among studies and limit our understanding of the underlying remodelling processes. Image analysis approaches, such as those that rely on two-dimensional Fourier transforms (6,7), have been developed to define a global fibre orientation distribution within an image, but these techniques lack the ability to localize regions of high fibre alignment, such as that found in a hypertrophic scar. Thus, establishing quantitative markers to objectively identify anomalies in collagen matrix formation remains a challenge in the laboratory and clinic.

Questions addressed

The goal of this study was to determine whether it is possible to quantify collagen fibre alignment and density from standard histological sections through automated image analysis approaches. To address this question, we have utilized a recently developed technique for the rapid quantification of fibre alignment at each pixel within images (8) and have integrated directional statistics with traditional image processing methods to create quantitative fibre organization maps for objectively characterizing scar remodelling following cutaneous burn injury.

Experimental design

To evaluate the wound healing response following burn injury, 6-week-old female Sprague–Dawley rats (Charles River Laboratories, Wilmington, MA, USA) were utilized. All animal procedures were performed in accordance with the guidelines of the National Institutes of Health (NIH) and approved by the Massachusetts General Hospital IACUC. Animals were anesthetized, and full-thickness third-degree burns (1 cm^2) were created on the dorsum by pressing a brass block preheated to approximately 95°C to the skin for 10 s as previously described (9). Tissue was harvested at 3 days, 1 week, 3 weeks, 2 months and 6 months after burn injury (n = 4/time point), as well as from uninjured control animals at 2 months. Tissue was processed, sectioned and stained with Masson's trichrome by the Rodent Histopathology Core at Harvard Medical School, and colour images of each tissue section were acquired using Hamamatsu's NanoZoomer Digital Pathology System (Hamamatsu, Japan) (20× objective, NA 0.75). Images were analysed by an experienced dermatopathologist (MCM).

Each trichrome tissue section image of approximately 18 megapixels (1.81 μm/pixel resolution) was analysed using custom-written code in Matlab (Mathworks, Natick, MA, USA). Collagen fibres that were stained blue were most clearly identified by a decrease in the transmission intensity in the red channel, and collagen-positive pixels were defined where the ratio of blue to red intensities exceeded 2 (Steps *ii* and *iii* in Figure S1). To minimize computational time, all images were automatically rotated and cropped to include only the collagen region of the dermis. Fibre orientation was computed with 2.5° accuracy at each pixel using the red channel of each image through a previously published algorithm that utilizes a weighted alignment vector summation technique within an 11 × 11 pixel window (8). To measure the relative local strength of fibre alignment, directional variance was computed at each pixel from all fibre orientations within a 50 pixel radius (Steps *iv*–*xi* in Figure S1). Similarly, to visualize the local fibre density surrounding each pixel, the relative fraction of collagen-positive pixels within a 50 pixel radius was calculated through spatial convolution with a disc kernel (Step *vii*). Parametric analysis using images from uninjured control and week 8 burn sections (Figure S2) guided the selection of the radius over which local fibre properties were calculated and the red:blue colour threshold to define collagen-positive pixels. Although additional increases in disc radius yielded modest improvements in scar discrimination (Figure S2), a 50 pixel radius was selected to retain the ability to identify local heterogeneity in tissue characteristics. Subregions of 300 × 700 μm corresponding to the wound centre, wound edge and uninjured adjacent tissue were predefined through blinded evaluation of the trichrome images (Fig. 1), and the average fibre density and directional variance within these discrete locations were computed. ANOVAs with post hoc Tukey HSD tests were used to assess differences among injury time points within each of these locations.

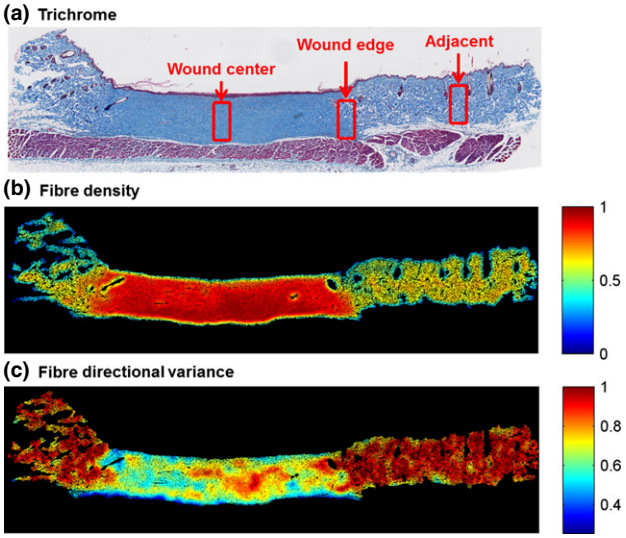

Figure 1. Fibre density and directional variance from a representative sample 6 months after burn injury. (a) Wound regions were manually selected within a 0.3 × 0.7 mm window delineating the wound centre, wound edge and an adjacent uninjured region. (b) Automated colorimetric analysis of each pixel enabled the identification of collagen-containing pixels, and collagen fibre density (processing step *vii* in Figure S1) measurements were significantly higher within the scar. (c) Pixel-wise fibre directional analysis enabled quantification of the local strength of collagen fibre alignment, and fibre directional variance (step *xi* in Figure S1) was significantly lower within the scar.

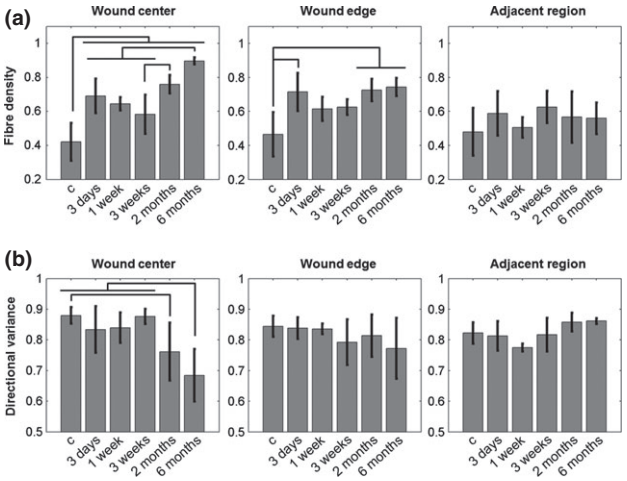

Figure 2. Quantification of fibre density and directional variance within different wound regions. (a) Fibre density in the centre of the burn wound was significantly elevated relative to control tissue, and significant increases in density were identified from 3 weeks through 6 months. Changes in fibre density with respect to time were attenuated at the wound edge, but significantly higher density was detected at 3 days, 2 months and 6 months relative to control. No differences in fibre density were detected in the regions adjacent to the wound. (b) Directional variance began to decrease after 3 weeks, with significant differences relative to control detected at 2 and 6 months. No significant differences in fibre alignment were detected at the wound edge or adjacent tissue.

Results

Following third-degree burn injury, an eschar was evident at 3 days and 1 week. In the time points that followed, a scar formed with no regeneration of sebaceous glands or hair follicles and collagen fibres increasingly aligned parallel to the skin surface. Both fibre density and directional variance were able to clearly delineate the scar region 6 months after burn injury (Fig. 1). A significant increase in fibre density and decrease in fibre directional variance were detected at the site of burn injury from 3 weeks through 6 months, indicating sensitivity to scar formation (Fig. 2, Figure S3). The centre of the wound contained a significantly greater fibre density at all postburn time points ($P \leq 0.0455$) compared to uninjured control tissue. After eschar detachment, fibre density was also greater ($P \leq 0.0315$) at 2 and 6 months relative to the 3-week time point (Fig. 2a). The variance of fibre directions in the centre of the wound was significantly lower at 2 and 6 months compared to control tissue ($P \leq 0.0488$), indicating an increase in fibre alignment (Fig. 2b). Directional variance at 6 months was also lower than all postinjury time points up to 3 weeks ($P \leq 0.0277$). The wound edge demonstrated similar, but attenuated, increases in fibre density over time, with no significant differences in directional variance (Fig. 2). Adjacent uninjured tissue regions did not significantly change relative to control with either metric (Fig. 2).

Conclusion

Automated pixel-wise analysis of fibre orientation within histology images enabled the quantification of increasing collagen fibre alignment and density during cutaneous scar formation after eschar detachment. This analysis technique offers a straightforward approach to track tissue remodelling and may provide objective surrogate endpoints for evaluating the collagen organization of human scar tissues in preclinical and clinical research.

Acknowledgements

This study was supported by NIH grant F32AR061933 to KPQ, American Cancer Society grant RSG-09-174-01-CCE to IG, NIH grant R01EB007542 to IG and Shriners Grant #85120-BOS to AG and MY.

Author contributions

KPQ developed the image analysis algorithms and analysed the data. AG, GFB, SK and MV designed the animal study and executed the experiments. MCM performed pathological analysis. WGA, BB, MLY and IG provided resources and guidance. All authors assisted in writing the manuscript.

Conflict of interests

The authors have declared no conflicting interests.

References

1 Kissin E Y, Merkel P A, Lafyatis R. Arthritis Rheum 2006: **54**: 3655–3660.
2 Agah A, Kyriakides T R, Lawler J *et al.* Am J Pathol 2002: **161**: 831–839.
3 Blackburn W R, Cosman B. Arch Pathol 1966: **82**: 65–71.
4 Bradshaw A D, Puolakkainen P, Dasgupta J *et al.* J Invest Dermatol 2003: **120**: 949–955.
5 Garcia-Gareta E. Exp Dermatol 2014: **23**: 473–474.
6 Ayres C E, Jha B S, Meredith H *et al.* J Biomater Sci Polym Ed 2008: **19**: 603–621.
7 Sander E A, Barocas V H. J Biomed Mater Res A 2009: **88**: 322–331.
8 Quinn K P, Georgakoudi I. J Biomed Opt 2013: **18**: 046003.
9 Golberg A, Broelsch G F, Bohr S *et al.* Technology 2013: **1**: 1–7.

Supporting Information

Additional supporting data may be found in the supplementary information of this article.

Figure S1. Overview of the collagen analysis algorithm.

Figure S2. Parametric analysis of variables used to quantify fiber density and directional variance.

Figure S3. Masson's Trichrome, fiber density maps and directional variance maps from representative samples at each time point.